A methodology for the detection of land cover changes: application to the Toulouse southwest region

Danielle Ducrot[1], Antoine Masse, Eric Ceschia, Claire Marais-Sicre, Daniel Krystof
Centre d'Etudes Spatiales de la Biosphère 18 av E.Belin - bpi 2801 - 31401 TOULOUSE cedex 9 France

ABSTRACT

A methodology to highlight changes in the landscape based on satellite image classification has been developed involving unsupervised and supervised approaches.

With past acquisitions, ground truth data are in general not known, therefore the classification can only be unsupervised. These classifications provide labels but not surface types. The main difficulty lies in the interpretation of these classes. An automatic interpretation method has been developed to allocate semantics to classes thanks to a radiometric value catalogue. However, it requires radiometrically comparable images. After radiometric correction, the images are not free from defects; this is why a normalization method has been developed.

We propose a specific methodology to evaluate changes consisting in regrouping classes of the same theme, smoothing and eroding contours without taking "mixels" into account and comparing the classified images to provide statistics and image changes. The different steps of the process are essential to avoid false changes and to quantify land cover change with a high degree of accuracy. Various statistical results are given: changes or no changes, types of changes, and crop rotations over several years.

Land use /cover change (LUCC) can provide an estimate of carbon capture and storage. Reforestation, changing land use and best practices can increase carbon sequestration in biomass and soils for a period of several decades, which may constitute a significant contribution to the fight against the greenhouse effect. Deforestation, conversely, can lead to significant levels of CO2 emission.

By application to the South-West region of Toulouse, we observe significant land cover changes over 11 years (1991-2002). The crop rotations are given for 4 years (year per year 2002-2005).

1. INTRODUCTION

Earth observation satellite images have been collected and stored for decades. Combining these satellite data, maps, geographical information systems and soil measurements, it is possible to improve the description of land surface states and processes. Data archiving enables the extension of analysis to the past and thus changes the way we analyze the landscape.

Land cover/use change detection has been a major field of application for remote sensing since the first earth observation satellite. Since remote sensing data from earth orbit can be obtained repeatedly over the same area, it has become useful to monitor and analyze land cover change. Several digital change detection algorithms have been developed ([8], [16]). Most change detection methods are based on the data sets collected at two different times. The time lapse between two data sets depends on the change characteristic investigated. Seasonal and annual changes of vegetation cover have been frequently analyzed by using vegetation indices derived from multitemporal data sets collected at more than 2 different times [12]. Certain change detection methods, such as band rationing and differencing, are primarily determined by the data sets that have constant environmental characteristics of atmospheric conditions and vegetation phenology.

Since it is difficult to maintain such constant environmental conditions among the multitemporal data sets to be analyzed, post-classification comparison methods are often used for analyzing land cover/use changes. They process each data set separately and only compare the classification results obtained from each data set [3]. However, this method assumes that the classification results are correct, which is not true in actual situations.

This study attempts to develop a methodology which limits uncertainties at different levels to define land cover change from multitemporal classification using post-classification methods.

[1] danielle.ducrot@cesbio.cnes.fr

The results from the land cover changes in Toulouse south west region and from crop rotation (every year for 4 years) will be used to determine carbon footprint (storage and emission).

2. UNSUPERVISED CLASSIFICATION AND AUTOMATIC INTERPRETATION

Ground truths are not always known, especially with old dates. The classification method can thus only be unsupervised. For land cover change detection, there are local variations depending on dates. Moreover, pixel-by-pixel classifications often have a salt and pepper appearance. This will induce false change. So, we have developed a fuzzy **contextual** algorithm of the ICM type (Iterative Conditional Mode) based on a Markovian model. This contextual method takes into account neighboring pixels [6]. We introduce segmentation to improve the contextual aspect of this ICM method. The applied segmentation algorithm is a multi-spectral temporal unsupervised process, so there is no need to select training data. This classification could be improved with the introduction of exogenic data such as GIS. Compared with traditional classification algorithms, ICM is robust and very open to the introduction of different rules, and can handle relatively complex and sophisticated relations among the spatial neighbor of the classes such as region given by segmentation. The same ICM principle is applied for supervised classification.

2.1. Interpretation methods

The partition of the image into N classes of unsupervised classification gives labels and not surface types. The main difficulty thus lies in the interpretation of the classes obtained by this kind of classification [12].

Visual method: In a traditional way, classification interpretation is visual and, therefore, manual with the assistance of radiometric image composite color. Using his knowledge, the interpreter deduces the allocation to a class. This is easy to recognize from form: forest, mineral surfaces/built, rivers. For crops it is more difficult because of their rotation. At certain times, using composite color, winter crops can be differentiated from spring crops in particular with infra-red or NDVI images.

Semi-visual method: For certain crops, a semi visual method is used to differentiate then by comparing their spectral and temporal signature with those of known ground truths from other years, but, preferably, after data normalization (see § 3 below). Indeed, radiometric values from different years must be comparable. This method is however relatively empirical, and the spectral /temporal signatures for certain classes to be interpreted do not really correspond to a particular class.

2.2. Interpretation by automatic recognition

An automatic recognition method was developed to assign semantics to unsupervised classification classes more systematically and less empirically. The interpretation is based on statistical radiometric values of classes established from ground truth samples from different years (average, standard deviation, minimum, maximum, covariance matrix). A class to be interpreted is assigned to the nearest class of a land cover catalogue of known thematic class, using several distances and divergences calculation. It is necessary to match anniversary dates of the satellite images (similar phenologic stage).

For each unsupervised class, the interpretation process assigns several distances: Bhattacharrya, Mahanalobis, Euclidean distance, and the maximum of probability with a Gaussian law, to the three most likely thematic classes. The definitive interpretation is given by rating these classes using a degree of certainty.

An example is given in table 1; the unsupervised classification statistics of 1991 are compared with those of 2002, 2003. For each unsupervised class the nearest thematic class is indicated on the first line for each statistical method (Bhattacharrya, Euclidean, and Maximum likelihood). Then, the next nearest classes are given in decreasing order. For example, in table 1, class 9 most frequently appears as a 1st choice, so the unsupervised class will be allotted to this class. The algorithm automatically computes the assignment to the “best” class with a confidence index.

We may note conflicts between several classes; in this case, the unsupervised class belongs to several thematic classes, so a special class is created. For example if a class contains wheat, rapeseed, we obtain the Wheat/Rapeseed class.

Confidence index: for each class the algorithm gives a certainty degree on its assignment, a number ranging between 0 to 1, 1 being the maximum certainty: for example, class 1 of the unsupervised classification of 1991, is assigned to class 9 (Sunflower) with a degree of certainty of 0.83.

Year	2002								2003							
Dist.	bhatta		euclid		likelihood		mahan		bhatta		euclid		likelihood		mahan	
Class 1 to interpret																
1st	9	2.084	9	246.79	9	74.316	9	4.083	12	1.625	10	245.294	10	65.389	12	3.6056
2nd	5	2.173	11	307.03	5	124.64	5	4.169	4	1.820	9	324.493	9	82.485	4	3.8158
3rd	4	2.236	10	326.56	8	128.72	4	4.229	20	1.881	20	365.058	8	89.576	20	3.8798
Class 2 to interpret																
1st	14	1.124	14	89.318	16	136.40	14	2.998	7	1.475	6	210.137	17	51.879	7	3.435
2nd	16	2.27	6	158.824	20	142.46	16	4.262	4	1.915	4	239.455	7	59.76	4	3.914
3rd	4	2.281	4	259.785	21	170.79	4	4.272	17	2.378	7	254.653	4	63.04	17	4.362
Class 3 to interpret																
1st	4	0.768	4	117.337	4	67.465	4	2.479	17	1.327	6	181.081	17	36.678	17	3.259
2nd	5	0.934	5	127.075	20	109.26	5	2.734	16	1.751	7	186.755	16	48.913	16	3.743
3rd	16	0.956	16	130.216	16	115.59	16	2.766	7	1.764	4	203.983	15	60.747	7	3.757

***Table 1**: automatic interpretation: divergences calculated with the 4 methods over 2 years (bhatta, eucli, maha: Bhattacharya Euclidean Mahanalobis distance, likelihood: maximum likelihood), the chosen number of reference class is followed by distance and divergence measurement.*

3. NORMALIZATION

Automatic interpretation needs to have comparable data. According to Bruzzone L., ([1], [2]), it is not possible to obtain a perfect alignment of multitemporal imagery due to the presence of local defects in images geometries. Consequently, residual misregistration results in inevitable additional noise, the "registration noise". It is essential to carry out the most efficient geometric and radiometric corrections to eliminate atmospheric effects and differences caused by the use of different sensors [18]. The method used allows estimating surface reflectance from Top Of Atmosphere (TOA) reflectance and the knowledge of the state of the atmosphere (water vapor, ozone and aerosol contents) [14].

After radiometric and geometric corrections, to minimize uncorrected radiometric disturbances and misregistration, a normalization method derived from Du et al [5], has been developed. This method is based on the assumption that the totality of disturbing effects can be approximated by linear functions. Pseudo-invariant features (PIFs) are used to determine the normalization coefficients. Multitemporal images of the same area are normalized to a common reference level based on the following formula:

$$Q_{ref}(i) = Q_j(i) * \alpha_i + \beta_j \qquad j = 1,2,3,\dots,m \tag{1}$$

Where *i* is the index of the PIF pixels, *j* is the index of the image, *m* is the total number of the images, Q_{ref} is the radiometric reference level, Q is the image value, α is the gain and β is the offset of the normalization.

The authors also describe an algorithm for statistical, semi-automatic selection of pseudo-invariant features (PIFs) on an image-to-image band-by-band basis. To determine PIF pixels and carry out the normalization, a bitemporal PCA is first applied to the same spectral bands of two different dates. The authors use manual thresholding to ensure the correct determination of the primary major axis. Pixels closest to the primary major axis are characterized by a strong linear interdependence thus are selected as PIF candidate pixels. After quality control of the resulting PIFs, transformation coefficients are calculated and a linear regression is performed to transpose radiometric values to the reference level. The regression coefficients can be determined by using known ground reflectances, PIF statistics of all image pairs, or one image as a reference. A post-normalization quality control step is also included in the method.

Some modifications and completions are implemented to enhance robustness mainly by decreasing manual interaction [10] and [11].

First, as mentioned above, pixels showing abrupt changes which are likely to influence the determination of the bitemporal PCA major axis have to be removed. Du *et al* [5] apply user-determined thresholds for each band to reject clouds and surface waters, and a difference threshold to reject pixels characterized by a large magnitude of change between the two dates. However, manual determination of thresholds for each band may be a time-consuming effort, and it includes subjective elements in the normalization process. Moreover, a simple difference threshold determines two parallel lines in 45° direction in the bitemporal scattergram, which can result in a loss of PIF candidate pixels at the highest and lowest values, if the principal major axis slope differs significantly from unity (Figure 1).

To ***enhance robustness and automaticity by using objective spectral*** difference measures and statistical thresholds, another method is developed and presented here. A multitemporal normalized band difference (MNBD) is calculated separately for each spectral band, with the following formula:

$$\mathrm{MNBD}_{xyi} = \frac{B_{xyi} - A_{xyi}}{B_{xyi} + A_{xyi}} \tag{2}$$

where MNBD is the normalized multitemporal band difference for the pixel with coordinates (x,y) of band i, A and B are geometrically rectified images of the same area taken at two different dates, A_{xyi} and B_{xyi} are the values of pixel with coordinates (x,y) of band i of image A and B, respectively. Note that the resulting MNBD image has a range between –1 and 1 with a sign depending on the order of the images in the numerator, and a symmetric distribution.

In the next step, mean and standard deviation (SD) of MNBD images is calculated, and then the values outside the interval [Mean ± *n* * Standard Deviation] are masked, where *n* is the selected MNBD threshold. The mean of MNBD values is chosen because in a first approximation, one can assume that atmospheric effects and anisotropic reflectance of surface elements lead to linear radiometric distortions, and that the distribution of landscape changes is symmetric. If there were no radiometric distortions, the mean value would be zero.

From a mathematical point of view, [Mean ± *n* * Standard Deviation] masking defines two lines starting from the origin of the multitemporal scattergram (Figure 2). The angle of the lines to the coordinate axes is defined by the MNBD mean value, while the angle between the two lines is defined by the standard deviation.

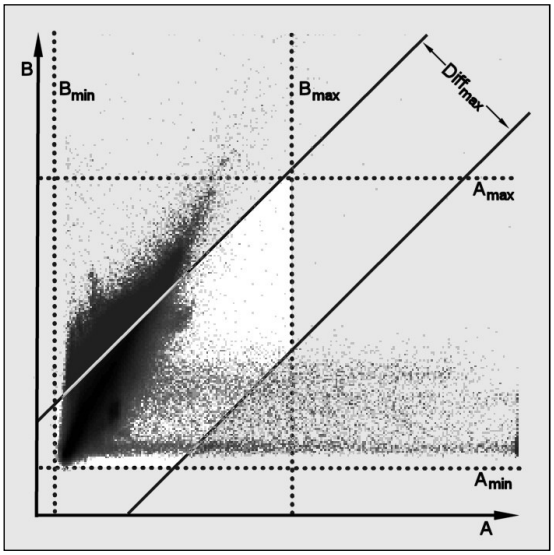

Fig 1: Multi-temporal scattergram showing the original method for pre-PCA pixel rejection on the radiometric values of two different image acquisition dates (A and B). Water and cloudy pixels are rejected using band-specific minimum and maximum thresholds (A_{min}, A_{max}, B_{min}, B_{max}). Pixels showing a large spectral difference between the two dates are also rejected using $Diff_{max}$ difference threshold. The remaining pixels (in the bright polygon) are used as PIF candidates. Note that a large number of possible PIF candidate pixels are lost, while cloudy pixels are kept.

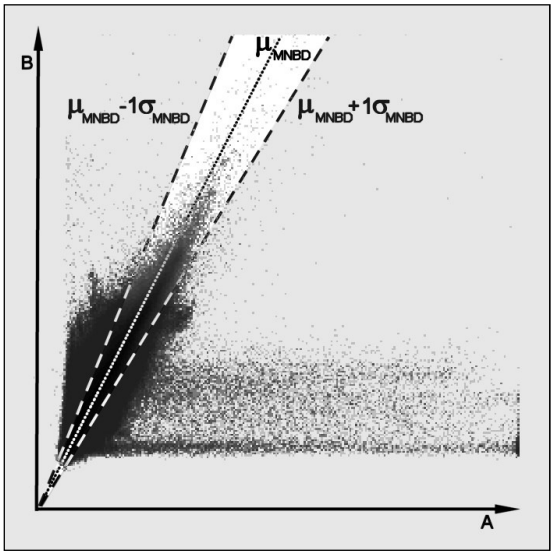

Fig 2: Multi-temporal scattergram showing the proposed method for pre-PCA pixel rejection on the radiometric values of two different image acquisition dates (A and B). Multi-temporal normalized band difference (MNBD) thresholds are determined statistically. Pixels showing an MNBD value close to the mean (μMNBD) are kept. Here, a one-standard-deviation (σMNBD) threshold is used. The majority of pixels containing clouds, local aerosol effects and other spectral changes are masked. The remaining pixels (in the bright triangle) are used as PIF candidates

After initial masking of abruptly changed pixels, all remaining pixels of the band pair are used in a bitemporal PCA, as described in [5], to obtain the two principal axes. The first principal axis contains unchanged pixels. Pixels with radiometric values within a range *l* from the primary major axis are selected by using statistical thresholds calculated from the second principal axis. The proposed algorithm is illustrated using multi-temporal scattergrams in Figures 3.

To determine the range *l* around the primary major axis to select PIF pixels, Du *et al* [5] use an iterative method with linear correlation coefficient (*r*) calculations as an internal quality control. They determine an initial range *l*, and calculate correlation coefficient for the pixels within the range ± *l* around the principal axis. They accept PIF candidates if $r \geq 0.9$; if not, radiometric and maximum difference thresholds as well as the range ± *l* along the primary major axis have to be improved. However, this procedure still contains subjective elements. Moreover, decreasing the range ± *l* leads to a strong decrease of the number of PIF pixels, while a high percentage of the image is an advantage of "no-change regression" methods; thus radiometric normalization errors are widely distributed across all major spectral classes [19]. With a sufficiently small value of *l*, a good correlation can be reached, but the final PIF accuracy and reliability can decrease due to the small number of PIF pixels.

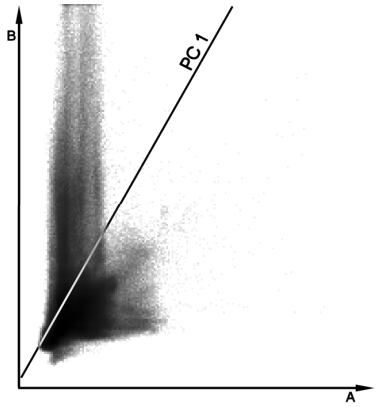

***Fig 3 a*:** Multi-temporal scattergram showing the effect of clouds, local aerosols and land cover changes on the determination of the principal axis. A and B are two different image acquisition dates, PC 1 stands for the principal axis. Note that PC 1 is determined erroneously due to cloud and land cover change effects.

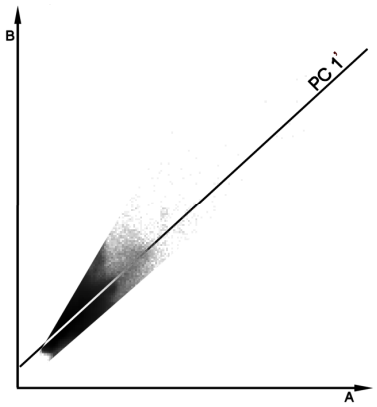

***Fig 3 b*:** PIF candidate pixels after mean +/- 1 Standard Deviation MNBD masking. PC 1' stands for the recalculated principal axis.

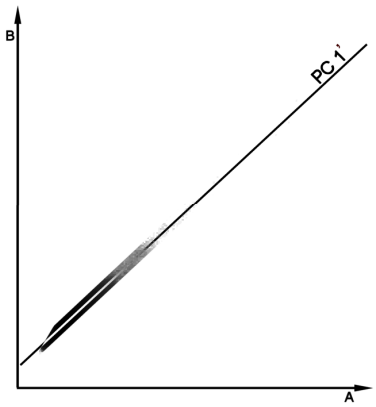

***Fig 3 c*:** PIF pixels after MNBD and mean +/- 0.5 SD second principal component masking. Pixels closest to the principal axis are determined and identified as PIFs. If the correlation criterion is met (R^2>0.95), PIF pixels are accepted.

Hence, the method is modified to be based on statistical calculations. Mean and standard deviation are calculated for the second principal band. PIF pixels are identified by the range of mean ± *m* standard deviations, where *m* is the selected threshold for principal component masking. Using statistical instead of rigid threshold, the extent of the second principal component (thus the multitemporal variability) is taken into account.

Linear correlation coefficient is then calculated for PIF quality assessment with a predetermined acceptance threshold; if this threshold is not reached, PIF selection has to be repeated with different MNBD and *l* values.

The next step is the calculation of normalization gains and offsets by using the statistics of the PIF pixels by the following equations (modified from [5]):

$$\text{gain}_{\text{BA}_i} = \frac{\sigma_{\text{A}_i}}{\sigma_{\text{B}_i}} \tag{3}$$

$$\text{offset}_{\text{BA}_i} = \text{m}_{\text{A}_i} - \frac{\sigma_{\text{A}_i}}{\sigma_{\text{B}_i}} * \text{m}_{\text{B}_i} \tag{4}$$

where $gain_{BAi}$ and $offset_{BAi}$ are the gain (α) and offset (β) from Equation (1) to convert the spectral band i of image B to the reference level A, σA_i and σB_i are the standard deviations of the PIF pixels in the spectral band i of the image B and the reference level A, respectively; σA_i and σB_i are the mean values of the PIF pixels in the spectral band i of the image B and the reference level A, respectively

A final step, by a new MNBD calculation, masking, and PCA of the corrected bands, the following method makes it possible to assess the normalization quality for individual images, as described in [5]. Slope of the principal major axis (SL) is calculated. The closer SL to unity, the better the normalization quality is considered to be.

However, it would be reasonable to evaluate the overall radiometric normalization quality over the time series; therefore, another method is suggested here. First, most stable PIFs are identified, (pixels that are selected as invariants (as described above) on all images of the time series in a given spectral band). For each of these PIFs pixels, the temporal standard deviation (SD) is calculated from the reflectance values of all dates; then, the average of these standard deviation values is computed. As the most stable PIFs are supposed to show constant reflectance over the entire period, the resulting spatial average of the temporal standard deviations corresponds to the "measurement error".

4. CHANGE DETECTION

The complexity of the change detection procedure depends on the characteristics of data sets. Selection of a single sensor series, low cloud cover and matching dates of two image data can restrict complexity and uncertainty. The difference between spatial resolution and spectral band of two image dates acquired with two sensors complicates direct comparison of data to detect changes [20]. The most common method that can be used to detect changes in multiresolution data sets is post-classification approach [3] and [4].

In the post-classification approach, images belonging to different annual dates are classified individually. The change detection step uses the processed information from classification, not the original data. The comparison of these individual classifications minimizes the problem of atmospheric and sensor differences amongst the image dates [16]. The classification results are then compared directly and the area of changes extracted [8], [16] and [20].

Accuracy dependence of the classification results is the main disadvantage of this method. Poor classification accuracy of individual classification leads to propagation of uncertainties in the change map, which results in inaccurate information of land-use changes. Shi *et al* [17] reported uncertainty propagation in classification-based change detection. The accuracy of the change product is the multiplication of the accuracies of the thematic maps: error of the source image, classification methods and determination of changes.

The change detection post-classification methodology proposed in this paper is ***supervised and unsupervised***. The steps previously described constitute the first part of the change detection system to minimize errors: fuzzy contextual classification, normalization and automatic interpretation. A specific protocol has been developed, as automatic as possible in order to better assess the changes. The principle consists in:

- ✓ groupings classes and sub classes to main categories according to the study goal. For example, we group forest classes and crops classes for CO2 storage and emission studies
- ✓ smoothing of the image to remove isolated pixels
- ✓ eroding contours to reduce the residual errors and not considering mixels
- ✓ comparing of classified images: cross-tabulating statistics: the algorithm provides a series of statistics according to the desired study theme, giving the percentages and areas of change or no change, and type of changes.
- ✓ creating the change map from the comparison, with possibly of dilating this image, to remove the eroded aspect of the image
- ✓ crop rotation over several years

4.1 Importance of contour erosion of the classification image

Based on the fact that most important misregistration effects can be observed at the edges of homogeneous regions, ***erosion eliminates pixels that form the border between two classes*** [19]. Depending on the satellite track, border pixels will be assigned to neighboring classes which may be different depending on the acquisition [15]. For example in the case of a bank at the edge of a river, the satellite collects an average of two classes (river and bank): the pixel can switch to the "bank" or to the river (river for one date, bank for another date, for the same scene). This is similar for all edge

pixels, which are mixed pixels (mixels). Contour erosion is necessary not to distort the statistics. The mixels are thus eliminated and the statistical results will be closer to reality. This also limits the problem of residual multitemporal shift (residual geometric errors).

4.2. Comparison of classified images from change matrices

Object-level change detection approaches can also minimize the effect of residual geometric errors. For example, Bruzzonne *et al* [2] and Jensen *et al* [7] improved change-detection accuracy with an adaptive parcel-based technique applied to small homogeneous regions shared by a multitemporal image pair. The object-based aspect is integrated in the contextual classification. Also, we compared parcel-to-parcel using the segmentation image; however in practice, agricultural parcels are sets of the same crop, which may vary for another year due to crop rotation. This generates statistical errors. In our case, more accurate results were obtained with pixel-by-pixel comparison.

If a class is different in the two classifications, a new class is a change class created. For example, a pixel allocated to the class "Wood" for one year becomes "Crop" for another year, then the class "Wood to Crop" will be generated. The algorithm presents various statistical results expressing class change in a matrix in terms of count and frequency (see example in table 2 & 3).

4.3. Crop rotation over several years

The method **compares N classifications of N years**, in order to follow landscape change and / or crop rotations or other rotation. The comparison is done automatically in several steps. The algorithm processes the first 2 images of the sequence, then the next image with the previous comparison result image. Thus we automatically obtain, the change matrix between all the images in terms of area and frequency: monoculture, annual biannual and triennial according to the years studied.

4.4. Land cover/use and carbon storage - emission

Carbon sequestration is the process by which growing trees and plants absorb CO2 from the atmosphere and turn it into biomass (e.g., wood, leaves, etc.). Deforestation, conversely, can lead to significant levels of CO2 emissions. [13].

The storage or emission of CO2 depends on the nature of the soil and its evolution of it over time. For example:

- Wood stores carbon, but differently according to its age and until saturation by CO2. Its absorption is maximal at the beginning and tends to decrease over time. Felling a tree, however, will release CO2 into the atmosphere.
- Absorption does not occur in the same way as it does in crops

Land cover/use can be used to calculate carbon footprint which involves studying the interaction between the biosphere and CO2 in order to better understand its storage capacity. Humane action through reforestation, changing land use, crop rotation and best practices can increase carbon sequestration in biomass and soils for period of several decades, which may constitute a significant contribution to the struggle against the greenhouse effect.

Satellite image land cover change mapping determines through classifications the storage and emission of CO2 in soil.

5. APPLICATION TO THE SOUTH-WEST REGION OF TOULOUSE (FRANCE)

Land cover change maps of the South-west of Toulouse were performed using classifications dating back to 1991 - 2002, then from classifications dating to 2002-2005 in order to study crop rotation. The satellite images provided by SPOT Image cover a surface of approximately 50*50 km². The landscape of this area is strongly impacted by human, with omnipresent crops.

5.1. Land cover changes from 1991 to 2002

For the year 1991, in the absence of ground truth, an unsupervised classification has been performed with three scenes from the satellite SPOT: May 22, August 3, and September 24, only available on the zone studied. Classes are automatically interpreted, thanks to 2002, 2003, 2004, 2005 ground truths.

5.1.1. Unsupervised classification interpretation of 1991 by automatic recognition

After normalizing the Spot images of 1991 with 2002 images, the automatic interpretation was performed.

The radiometric values of 1991 classes are compared with those of the reference classes (2002, 2003, 2004), at the same phenologic stage (nearest possible date), thanks to calculations of multi spectral -temporal distances and probability (see § 2) with the reference sample sets. Thus, a class to be interpreted is assigned to a known thematic class from our land cover catalogue.

The three dates are sufficient to discriminate between six classes corresponding to main land cover categories (Wood, Winter Crops, Summer Crops, Meadow, Fallow, Water and Mineral Areas). The distribution of these principal classes is expressed in proportion to the entire studied zone: Wood 12.83%, Winter crops 17.24%, Summer crops 48.475%, Meadows 6.478%, Fallow /Waste lands 12.669%, Mineral areas 2.23%.

5.1.2. Supervised classification (2002)

Spot images supervised classification of 2002 produces a map of 16 land cover classes: wooded formations (Leafy trees, Coniferous tree, Eucalyptus), crops (Wheat, Barley, Rapeseed, Corn, Sunflower, Sorghum, Soybean, Pea), grassland (Meadows and Fallow), water (River, Lake, Gravel pit) and Mineral surfaces/Built. Classification precision given by the confusion matrix using checking samples gives an accuracy of 87.4% and Kappa of 88.7% (we obtain higher percentages with training samples). After image smoothing, grouping 2002 classes identically to 1991 and edge erosion, the classifications are compared (1991 - 2002) and thereby giving the description of land cover change.

5.1.3. Land change analysis

The established protocol consists in determining what class replaces what class. The outcomes are expressed as change matrices and a map. Land change analysis provides various statistics levels related to the land cover management mode. For example, conversion from:

- ✓ Crop 1 to Crop 2 does not change the land, it only concerns agricultural practice (crop rotation);
- ✓ Crop to Meadow / Fallow may reflect the influence of agricultural policy (land fallow mandated by the 1992 CAP (***common agricultural policy***))
- ✓ Crop to Wood or Mineral surfaces/built indicates a net change of land use planning indicating decline of the UAA (Utilized Agricultural Area) under the influence of various pressures of socio-economic development.
- ✓ Wood to another class belonging to a new category of non-forested land (crop or mineral surfaces/built) indicates a deeper change of allotment of space. We must therefore seek the cause or determinants to measure the impact in terms of landscape and ecology.

	Classification 2002					
Classification 1991	Wood	Winter crop	Summer crop	Fallow	Meadow Grassland	Mineral Surfaces/built
Wood	**70.89**	2.51	3.01	10.40	10.72	0.09
Winter crop	0.12	**41.99**	42.04	2.32	12.37	0.09
Summer crop	0.47	32.56	**53.79**	2.12	10.03	0.15
Fallow	1.02	12.35	14.37	**6.60**	61.90	0.06
Meadow-Grassland	0.65	13.18	17.84	2.72	**65.18**	0.07
Meadow-Grassland/Fallow	8.00	20.58	25.60	7.19	36.26	0.12
Mineral Surfaces/built	2.64	2.38	4.67	2.78	7.15	**61.17**

Table 2: Changes matrix (frequencies) (1991-2002)

Changes over this 11 year period are significant. They make it possible to highlight facts evolution trends of the regional landscape influenced by the policies of land management: we observe a slight retreat of the Wood class and an increase of Grassy surfaces (table 2 & 3).

5.1.3.1. Stability: 77.97% of land between 1991 and 2002 does not change

- ✓ 70.09% of the Wood class is unchanged, which represents 8.17% of the area
- ✓ 84.71% of the Crop is unchanged at 57.41% of the area
- ✓ 54.62% grassed surfaces unchanged, 9.59% of area, 38% went to the crops, or 6.67% of area

Surfaces do not include the eroded areas.

Classes unchanged		Numbers	Surface ha	**Land cover (%) in the resulting change image**	**Classes changed or not (%) 1991 versus 2002**
Wood		181925	7277.00	8.273	70.89
Crop		1234114	49364.56	***56.121***	85.42
Grassy land		178077	7123.08	8.098	53.79
Water		11684	467.36	0.531	
Mineral Surface / Built		27343	1093.72	1.243	55.95
total unchanged			***65325.72***	***74.266***	
1991	***Changes (2002)***				
Wood →	Crop	18939	757.56	0.861	5.52
	Grassy land	54214	2168.56	2.465	21.12
	Mineral Surface / Built	6105	244.20	0.278	2.38
	Total conversion wood	79258	***3170.32***	***3.604***	***29.54***
Crop →	Grassy land	190295	7611.80	***8.654***	13.17
	Mineral Surface / Built	13764	550.56	0.626	2.47
Grassy land →	Wood	16829	673.16	0.765	5.08
	Crop	127983	5119.32	***5.820***	38.66
	Mineral Surface / Built	8194	327.76	0.373	2.47
Mineral Surface / Built →	Wood	369	14.76	0.017	0.76
	Crop	14154	566.16	0.644	29.05
	Grassy land	6863	274.52	0.312	14.08
Green urban area →	Wood	781	31.24	0.036	0.80
	crops	41626	1665.04	1.893	42.55
	Fallow, Meadow	42957	1718.28	1.953	43.91
Diverse				1.09	
Total changes		2176622	***21739.16***	***24.715***	

Table 3: frequencies are related to the image changes over the surface of the image compared to the surface of this image (without the eroded area)

5.1.3.2. Changes (approximately 22%)

- ✓ Wooded surfaces suffer 30% change mainly to grassy surfaces (22.6%), 3.6% of area image; this concerns mainly small patches and field wooded borders than forest. The rest of conversion is negligible.
- ✓ Conversion to wooded areas by crop is negligible. We note some plantations, wooded areas into peri-urban, young plantations which have grown.
- ✓ Crops are most stable, 13.79% have change to grassy surfaces (8.6 %of the area). But Fallow and Meadow fits into the crop rotation cycle. There are more grassy surfaces to crop change than the reverse. Culture to Meadow / Fallow may reflect the influence of agricultural policy (land fallow mandated by the 1992 CAP (common agricultural policy)). But these results must be moderated: all kinds of grassy lands Fallow and Meadow, Waste lands, are very similar radiometrically, they are difficult to distinguish. Some of these changes are due to confusion between these classes. Note that the class "Meadow / Grass" may contain lawns, parks.....

- ✓ Conversion to grassy areas has occurred from every class.

- ✓ Urbanization: a emerging of urbanization is noticed: 1.95% of the Crops classes, Wooded area, Meadows, Fallow, Wood
- ✓ Mineral surfaces/Built class sees its surface growing by approximately 1.5%. This class includes roads, bare soil, sometimes confused with winter crop stubble, if the date of March or April does not exist.

5.2 Evolution of the land cover between 2002 and 2005; crop rotation 2005 → 2004 → 2003 → 2002

The same principle as before was applied for the study of the change between 2002 and 2005. For these years, classifications are supervised.

As previously, main changes are evaluated:

- conversion Forest to Crop, Meadow to Crop (and vice versa), these change are important for storage or emission of atmospheric carbon
- Mineral surfaces/Built in order to estimate a possible urbanization.

During this period, the change frequencies are low except for Fallow which varies with Meadow, but we know that these two classes are often confused. Crops remain stable; urbanization is not yet very intense except near Toulouse. The forest, main subject of study for carbon storage, does not show very significant changes.

2002 → 2003→ 2004 → 2005	Pixel number 2002→ 2003→ 2004→ 2005	area (ha)	Percentage = class pixel number/total pixel number of the eroded image	2002 → 2003 → 2004 → 2005	Pixel number 2002→ 2003→ 2004→ 2005	area (ha)	Percentage = class pixel number/total pixel number of the eroded image
monoculture				**Every 3 years** (main changes)			
Corn-Corn-Corn-Corn	136422	5456.8	**6.339**	Wheat-Wheat-Wheat-Sunflower	84391	3375.64	3.922
Wheat-Wheat-Wheat-Wheat	8891	355.64	0.42	Corn-Corn-Corn-Wheat	22440	897.6	1.043
Soybean-Soybean-Soybean-Soybean	58	2.32	0.003	Corn-Corn-Corn-Sunflower	21931	877.24	1.019
Sunflower-Sunflower-Sunflower-Sunflower	1931	77.24	0.09	Sunflower-Sunflower-Sunflower-Wheat	17116	684.64	0.795
2 crops				Wheat-Wheat-Wheat-Rapeseed	13859	554.36	0.644
Bi-annual (main changes)				Corn-Corn-Corn-Soy	10682	427.28	0.496
Wheat-Sunflower-Wheat-Sunflower	402924	16116	**18.72**	Wheat-Wheat-Wheat-Corn	10483	419.32	0.487
Wheat-Corn-Wheat-Corn	29262	1170	1.36	Wheat-Wheat-Wheat-Corn	10483	419.32	0.487
Every 2 years							
Wheat-Wheat-Sunflower-Sunflower	30826	1233.0	1.43				
Wheat-Wheat-Corn-Corn	8153	326.12	0.38	**Rotation**			
Corn-Corn-Sunflower-Sunflower	3393	135.72	0.16	**Total 2 crops**	***690170***	***27606.8***	***32.07***
Corn-Corn-Soy-Soy	592	23.68	0.03	**Total 3 crops**	***210847***	***8433.88***	***9.8***
Soybean-Wheat-Wheat-Soybean	435	17.4	0.02	**Total 4 crops**	***7937***	***317.48***	***0.37***

Table 4: crop rotations: monoculture, biannual, triennial …

Crop rotation

For crop rotation study, the crops are not grouped: they are considered independently. The principle of change comparison in land use of the four images: 2002, 2003, 2004 and 2005 is the following:

1. 2002 image compared to 2003, the results are: a change image 2002- 2003 and a change matrix.

2. The resulting 2002-2003 image is compared with the 2004 classification and the result is a change image 2002-2003-2004, with its change matrix

3. The 2002-2003-2004 resulting image is compared with the 2005 classification and the result is the image changes 2002-2003-2004-2005, and its change matrix

Resulting images cannot be displayed, the limit is imposed by its classes number, which exceed the 255 classes for maximum screen viewing (they must be grouped) .The algorithm mainly keeps the significant changes and statistics on the land rotations.

The most important rotations are those of Wheat which generally rotates every year mainly with Sunflower. Rapeseed and Barley change every year (*table 4*).

Results

- **monoculture** is mainly **Corn**; it covers **6.34**% of the territory, the others are negligible
- Main rotation: Wheat and Sunflower: biannual rotation (20% of eroded surface with 18.7% Wheat-Sunflower)
- ***32%*** are occupied by crops of 2 types (mainly Sunflower and Wheat) in rotation from 1 to 4 years
- ***9.8%*** of rotation out of 3 crops
- rotation with 4 crops is negligible

6. CONCLUSION

Accurate change statistics over several years can be obtained here using the protocol presented …. Every step is important: fuzzy contextual classification, automatic interpretation of the unsupervised classification, edge erosion of the classification. Results are facilitated depending on image acquisition conditions. Selection of a sensor series, low cloud cover and matching dates of two image data can restrict uncertainty. It is essential to choose appropriate calendar acquisition dates to obtain correct results. On the other hand, on anniversary dates, phenological discrepancies due to local precipitation and temperature variations can appear as well [4].

This protocol was first tested on areas where we had ground truths. The overall PCC (pixel corrected classes) were improved with respect to direct comparison classification. Change statistics have been verified with agricultural European agency statistics and state agency statistics. The advantage of these statistics is they provides ***quantitative measurements***, particularly rotations statistics.

Land cover changes from wood, crop, fields are important to evaluate the emission and storage of CO2, which depend on the nature of the soil and its changes over time. For example: wood stores carbon, while the cutting of a tree will release CO2 into the atmosphere. Absorption does not occur in the same way in wood and in crops.

In post-classification change detection analysis, the minimization of classification errors is fundamental. Thus further work will be requires to improve the fuzzy contextual method presented. In the case of unsupervised classification, the improvements will be in automatic interpretation.

REFERENCES

[1] Bruzzone, L., Cossu, R., “An Adaptive Approach to Reducing Registration Noise Effects in Unsupervised Change Detection”, IEEE Trans. Geosci. Remote Sensing, vol. 41, no. 11, pp. 2455-2465 (2003).

[2] Bruzzone, L., Fernandez Prieto, D., “An adaptive parcel-based technique for unsupervised change detection”, Int. J. Remote Sensing, vol. 21, no. 4, pp. 817-822 (2000).

[3] Castelli, V., C. D. Elvidge, C. S. Li and J. J. Turek. “Classification-based change detection: Theory and applications to the NALC dataset. In Remote sensing change detection:environmental monitoring methods and applications”, edited by R.S. Lunetta and C. D. Elvidge.London, UK: Taylor & Francis, 53-73 (1999).

[4] Coppin, P., Jonckheere, I., Nackaerts, K., & Muys, B., "Digital change detection methods in ecosystem monitoring: a review", Int. J. Remote Sensing, vol. 25, no. 9, pp. 1565-1596 (2004).

[5] Du, Y., Teillet, P. M., Cihlar, J., "Radiometric normalization of multitemporal high-resolution satellite images with quality control for land cover change detection", Remote Sens. Environ, 82:123-134 (2002).

[6] Idbraim, S., Ducrot D. , "An unsupervised classification using a novel ICM method with constraints for land cover mapping from remote sensing imagery", International Review on Computers and Software (IRECOS), vol 4 N.2 (2009).

[7] Im, J. and Jensen, J. R. ,"Object-based change detection using correlation image analysis and image segmentation" , International Journal of Remote Sensing Volume 29 , Issue 2 Pages: 399-423 (2008).

[8] Jensen J.R., "Introductory Digital Image Processing: A Remote Sensing Perspective" , 2ndEdition, Prentice-Hall, Upper Saddle River, NJ (1996).

[9]Ji M. , "Using fuzzy sets to improve cluster labelling in unsupervised classification ", International Journal of Remote Sensing, Volume 24, Issue 4 , pages 657 - 671 (2003).

[10] Kristóf, D., Ducrot D., "Environmental Impact Assessment of a Barrage System Using Novel Change Detection Methods", Proceedings of the IGARSS '03 Symposium IEEE, (2003).

[11] Kristóf, "Application de la télédétection pour la cartographie et le suivi des écosystèmes forestiers – application à la forêt hongroise", Thesis, (2005)

[12] Lambin, E.F. and D. Ehrlich, "Land-cover changes in sub-Saharan Africa (1982-1991): Application of a change index based on remotely sensed surface temperature and vegetation indices at continental scale", Remote Sensing of Environment, 61-:181-200 (1997).

[13] Poussart, J.N., Ardö, J., Olsson, L., "Verification of soil carbon sequestration – sample requirements", Environmental Management, DOI: 10.1007/s00267-003-9149-7 (2004).

[14] Rahman, H., and G. Dedieu, SMAC A, "Simplified Method for the Atmospheric Correction of Satellite, Measurements in the Solar Spectrum", Int. J. Remote Sens., 15 (1), 123-143 (1994).

[15] Serra P. , Pons X. , Saur D. , "Post-classification change detection with data from different sensors: some accuracy considerations", I J R S, Vol24, Issue 16 , p3311 – 3340 (2003).

[16] Singh, A. , "Review Article: Digital change detection techniques using remotely-sensed data", Int. J. , Remote Sensing, 10(6), 989-1003 (1989).

[17] Shi, W.Z. and M. Ehlers, "Determining uncertainties and their propagation in dynamic change detection based on classified remotely-sensed images", Int. J. Remote Sensing, 17(14), 2729-2741, References 49, (1996)

[18] Song, C., Woodcock, C. E., Seto, K. C., Pax Lenney, M., & Macomber, S. A., "Classification and Change Detection Using Landsat TM Data: When and How to Correct Atmospheric Effects?" ,Remote Sens. Environ, 75:230-244 (2001).

[19] Stow, D. A. , " Reducing the effects of misregistration on pixel-level change detection",. Int.J.Remote sensing, 20(12), 2477-2483 (1999).

[20] Yuan, D., & Elvidge, C. D., "Comparison of relative radiometric normalization techniques", ISPRS Journal of Photogrammetry & Remote Sensing, 51:117-126 (1996).